Supporting Information

Effects of Substrate and Polymer Encapsulation on CO_2 Electroreduction by Immobilized Indium(III) Protoporphyrin

Yuvraj Y. Birdja,[†] Rafaël E. Vos,[†] Tim A. Wezendonk,[‡] Lin Jiang,[†] Freek Kapteijn,[‡] and Marc T. M. Koper*[,†]

†*Leiden Institute of Chemistry, Leiden University, PO Box 9502, 2300 RA Leiden, The Netherlands*

‡*Catalysis Engineering, Chemical Engineering Department, Delft University of Technology, Van der Maasweg 9, 2629 HZ Delft, The Netherlands*

E-mail: m.koper@chem.leidenuniv.nl

Materials and Experimental procedures

Materials

Pyrolytic graphite (PY001009, Graphite Store, USA), cut in 5 mm diameter discs such that the basal planes are exposed, glassy carbon (5 mm diameter) and boron doped diamond (10 mm diameter, Windsor Scientific Ltd., UK) were used as working electrode.

Potassium phosphate dibasic TraceSELECT $\geq$99.999% (Honeywell) and potassium phosphate tribasic (Sigma Aldrich) were used for the preparation of the phosphate buffer solution of pH = 9.6 $\pm$ 0.1. The pH was measured with a SI Analytics Lab 855 pH meter. The Indium(III) protoporphyrin IX was purchased from Frontier Scientific and used without further purification.

The chemicals used for immobilization in polymer membranes were didodecyldimethylammonium bromide (98 %, Sigma Aldrich), Nafion® perfluorinated resin solution (5 wt. % in lower aliphatic alcohols and water, contains 15-20% water, Sigma Aldrich), poly(4-vinylpyridine) (average Mw $\approx$ 60,000, Sigma Aldrich) and poly(3,4-ethylenedioxythiophene)-poly(styrenesulfonate) (0.54% in H_2O, high-conductivity grade, Sigma Aldrich)

Electrochemical experiments

Glassware was cleaned as in our previous work.[1] Prior to each experiment, the PG and GC electrodes were polished and ultrasonicated in water for approximately 5 min in water. PG was polished with sandpaper (first P600 and then P1000), and GC with alumina slurry (1μm, 0.3μm and 0.05μm particle size). BDD was first ultrasonicated in concentrated nitric acid for 5 min and then in water. The subsequent procedures (deaeration of the cell, voltammetric procedures before and after InPP immobilization) are akin to the procedures reported previously.[1]

Product analysis

High Performance Liquid Chromatography (Prominence HPLC, Shimadzu) was utilized for the analysis of non-volatile reaction products. The samples were placed in an auto-sampler (SIL-20A) which injects 20 μl of the sample into the column. An Aminex HPX 87-H (Bio-Rad) column with a Micro-Guard Cation H Cartridge (Bio-Rad) in front were used. The eluent was 5 mM H_2SO_4 and the eluent flow rate 0.6 ml min^{-1}. The column and the refractive index detector (RID-10A) were maintained at a temperature of 45 °C. The setup utilized for online HPLC experiments has been described before.[2]

OnLine Electrochemical Mass Spectrometry (OLEMS) was utilized for the detection of volatile reaction products. A tip, containing a hydrophobic membrane is placed close (≈10 μm) to the electrode surface, and continuously collects volatile reaction products from the electrode interface. The setup has been described previously.[3]

Immobilization of InPP

The immobilization of InPP onto the substrate was performed by dropcasting 2.5 μl 0.25 mM InPP solution per 0.196 cm^2 geometric surface area, followed by evaporation of the solvent under an argon stream. The preparation of the InPP solution has been described by de Groot et al.[4] For the experiments on the substrate effect and pretreatment effect the immobilization was consistently carried out with InPP in DDAB layers, as this resulted in higher activity. For investigation of the polymer effect, InPP was also dropcasted without polymer from the solution reported by de Groot et al. The immobilization using Nafion, P4VP and PEDOT:PSS were carried out similarly with minor modifications. The InPP-Nafion and InPP-PEDOT:PSS solutions were prepared by mixing equivolumes of 0.5 mM InPP stock solution with respectively 2 wt.% Nafion solution or 0.54 wt.% PEDOT:PSS solution. Due to the insolubility of P4VP in the InPP stock solution, we first dropcasted 0.5 mM InPP solution on PG, followed by an equal volume of 2 wt.% P4VP solution (in 0.1 M acetic acid). For a correct comparison, it was made sure that the amount of dropcasted

InPP per cm^2 is always the same.

Pretreatment of pyrolytic graphite

The electrochemical pretreatments of the pyrolytic graphite surface were carried out in a conventional one-compartment three electrode cell with 0.1 M perchloric acid (Merck Suprapure) electrolyte. A platinum wire was used as counter electrode and reversible hydrogen electrode as reference. For the anodic pretreatment, chronoamperometry at E = 2.25 V vs. RHE for t = 5 minutes was performed, and for the cathodic pretreatment, chronoamperometry at E = -1.8 V vs. RHE for t = 5 minutes.

For the plasma treatment of the pyrolytic graphite electrodes a capacitively coupled plasma system with the Radio-Frequency (RF) of 40 kHz and 200W power from Diener electronic was employed at room temperature. The base pressure of this system is less than 0.02 mbar. The parameters were 10 W power/1.0 mbar pressure for H_2 plasma and 30 W power/0.5 mbar pressure for O_2 plasma. For H_2 the exposure time was 3 minutes, and for the O_2 plasma we varied the exposure time (3, 6 and 12 minutes) to achieve mild and harsh plasma treated PG.

Apparatus

X-ray diffraction data were collected on a Philips X'Pert diffractometer, equipped with the X'Celerator, using Cu-Kα radiation in steps of 0.02° (2θ) with 10 s counting time in the range from 10° to 80° (2θ).

Raman spectra were recorded with a WITEC alpha300 R – Confocal Raman Imaging spectrometer with a laser wavelength of 532 nm at ambient conditions and room temperature.

X-ray photoelectron spectroscopy (XPS) measurements were performed on a K-alpha Thermo Fisher Scientific spectrometer using a monochromated Al Kα X-ray source. The measurements were carried out using point analysis with auto-height signal optimization, with each point having a spot size of 300 micron at ambient temperature and chamber

pressure of about 10^{-8} mbar. A flood gun was used for charge compensation. All the measured spectra were corrected by setting the reference binding energy of C*1s* at 284.8 eV. The electron energy analyzer was operated with pass energy of 200 eV and 0.25 eV energy spacing for the survey spectrum, and pass energy of 50 eV and 0.1 eV energy spacing for the high-resolution spectrum. Each reported spectrum is the statistic average of 10 measured scans. To ensure homogeneity of the immobilized InPP, different spots of the samples were analyzed. The spectra were analyzed and processed using Thermo Avantage v5.903 software (Thermo Fisher Scientific). Smart background subtraction, derived from the Shirley background, was used over the peak width. By applying full width integration over the core-level signals and using tabulated atomic sensitivity factors, relative atomic contributions on the surface were calculated.

Substrate effect

In the Figures S1-S3 we compare the influence of different amounts of InPP on PG, GC, and BDD on the selectivity and activity of CO_2RR. The amount InPP per cm^2 is kept the same for all the substrates. For PG we observe that a higher amount of InPP on the surface leads to a significant increase in FE and j_{HCOOH}, and decrease in j_{H_2}, while j_{total} remains unchanged. These observations are associated with the higher amount of active sites available, where even an initial FE of approximately 100 % can be obtained. Conversely, as can be seen in Figure S2, on GC a higher amount of InPP has negligible influence on CO_2RR selectivity and activity. In terms of FE, BDD is somewhat in between PG and GC, but the HCOOH activity seems to be inhibited for higher InPP concentrations. These results show the different behavior of the substrates with increasing amounts of dropcasted InPP, which is interpreted as the capacity of PG to accommodate more InPP compared to GC and BDD. In order to draw more quantitative conclusions, we performed XPS measurements on the different substrates with immobilized InPP. XPS is a very useful and sensitive technique to study the surface species. In Figure S12, the XPS spectra of the different substrates with and without InPP are shown. As reference for the indium protoporphyrin, the spectrum of $In_2(SO_4)_3$ is included as well. Analysis of the XPS spectra of InPP containing substrates and $In_2(SO_4)_3$ indicate a clear In(III) contribution with peak broadening of In*3d* core level binding energy. No loss of features at higher binding energy is observed, indicative of absent metallic In species. The indium content extracted from the XPS spectra is used as a quantitative measure for the real amount of adsorbed InPP on the substrates.

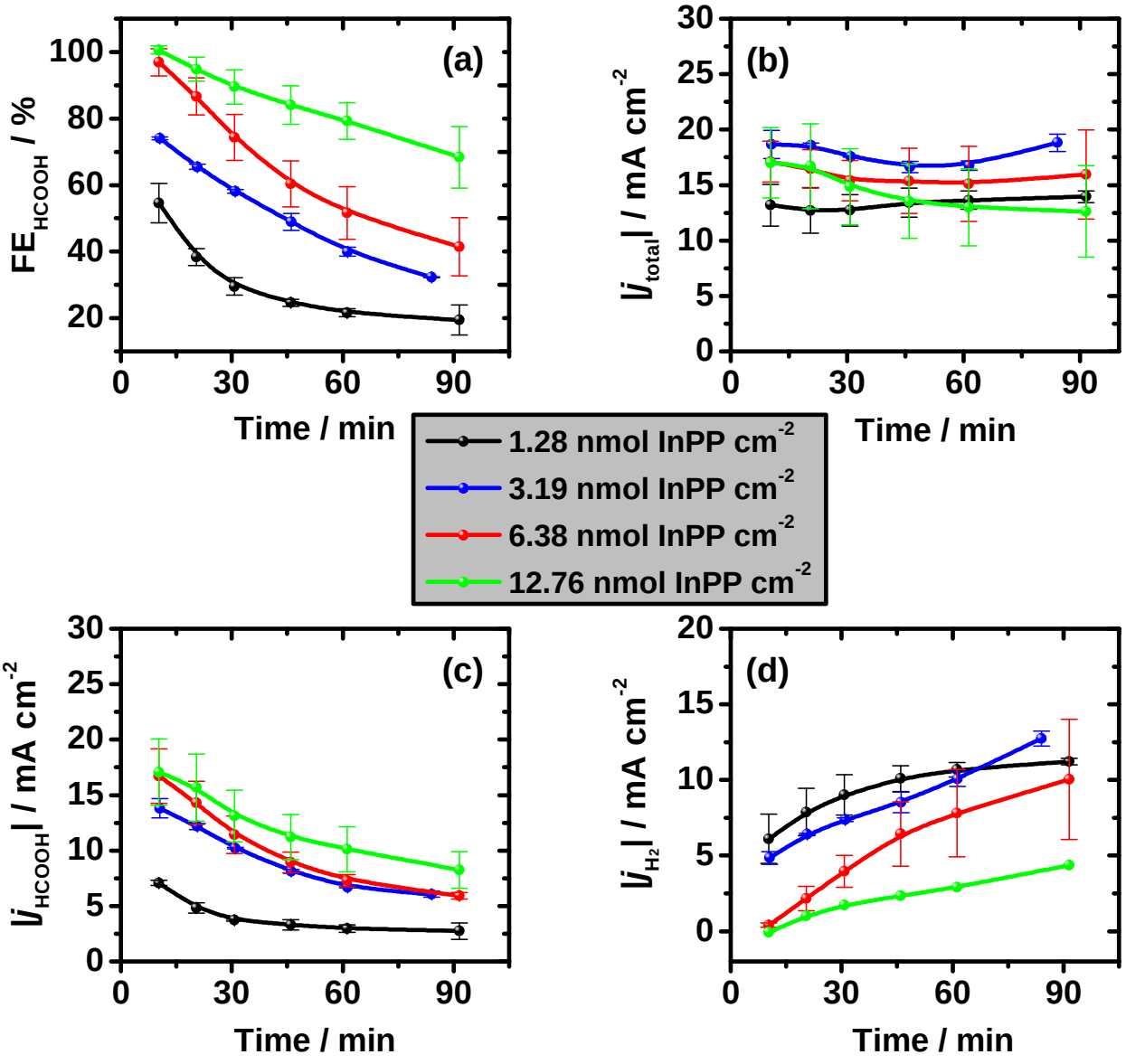

Figure S1: (a) Faradaic efficiency toward HCOOH, (b) absolute total current density, (c) absolute partial current density for HCOOH, (d) absolute partial current density for H_2 during CO_2 reduction on different amounts of immobilized InPP on PG in 0.1 M phosphate buffer of pH 9.6. Lines to guide the eye.

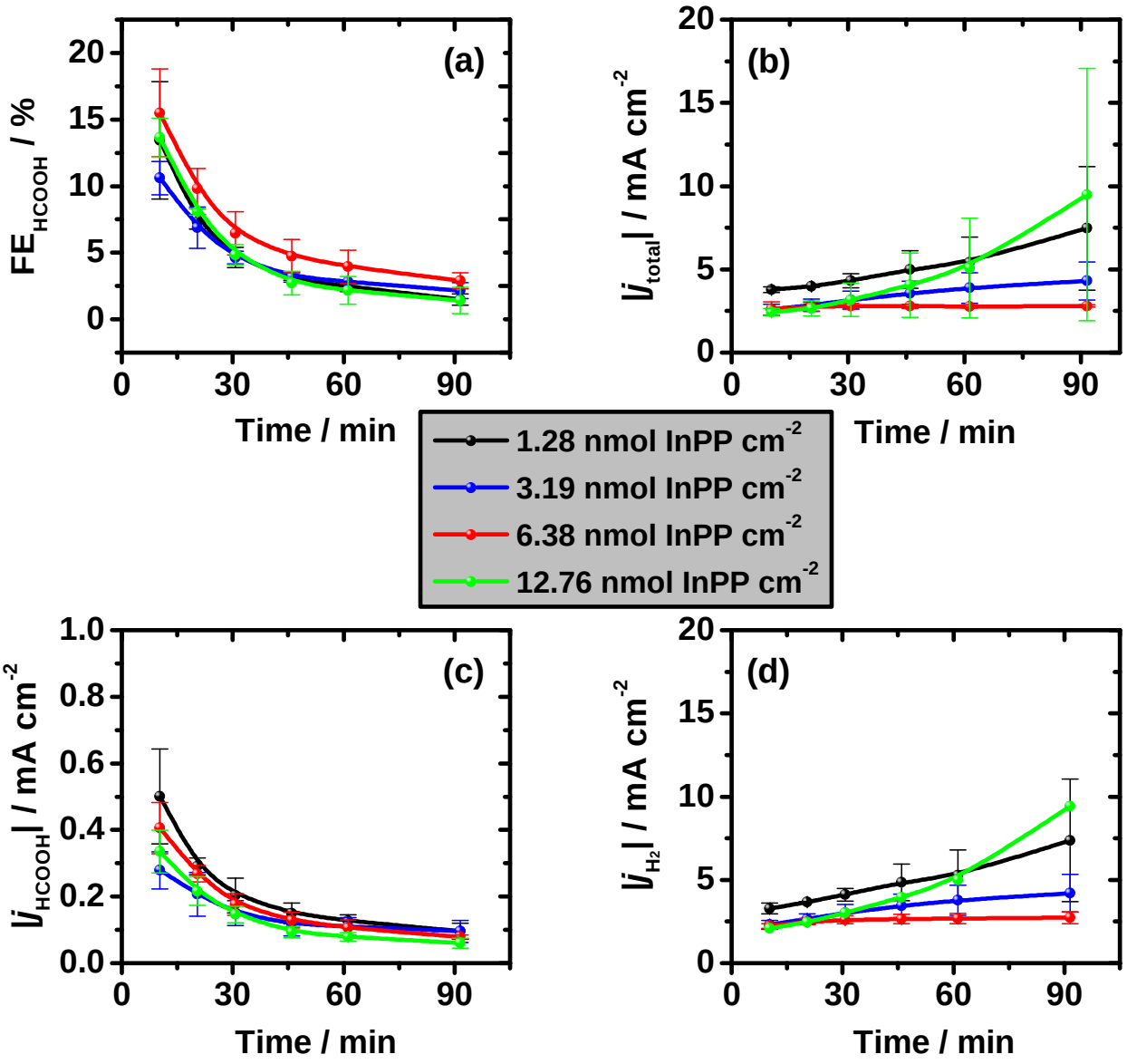

Figure S2: (a) Faradaic efficiency toward HCOOH, (b) absolute total current density, (c) absolute partial current density for HCOOH, (d) absolute partial current density for H_2 during CO_2 reduction on different amounts of immobilized InPP on GC in 0.1 M phosphate buffer of pH 9.6. Lines to guide the eye.

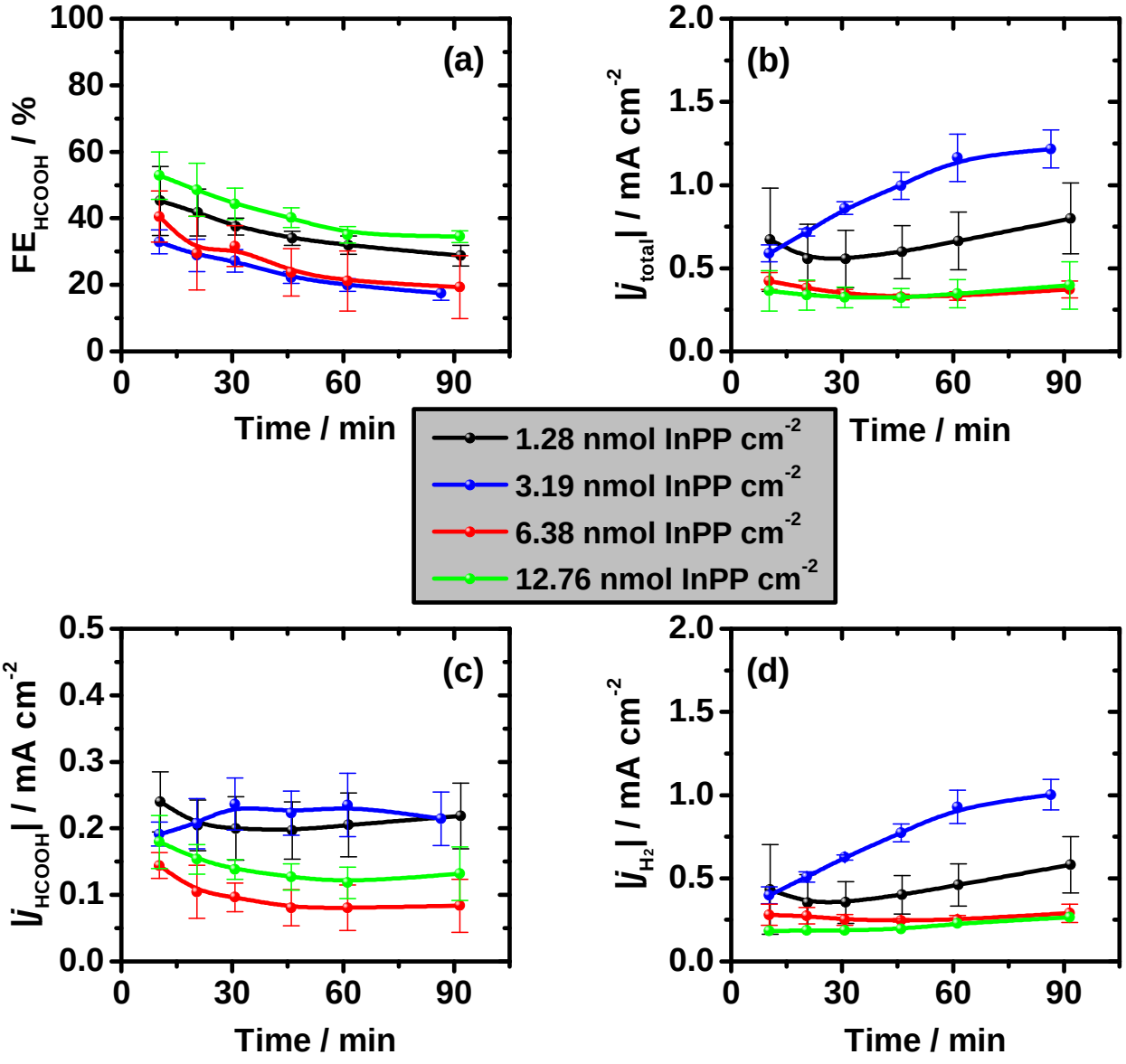

Figure S3: (a) Faradaic efficiency toward HCOOH, (b) absolute total current density, (c) absolute partial current density for HCOOH, (d) absolute partial current density for H_2 during CO_2 reduction on different amounts of immobilized InPP on BDD in 0.1 M phosphate buffer of pH 9.6. Lines to guide the eye.

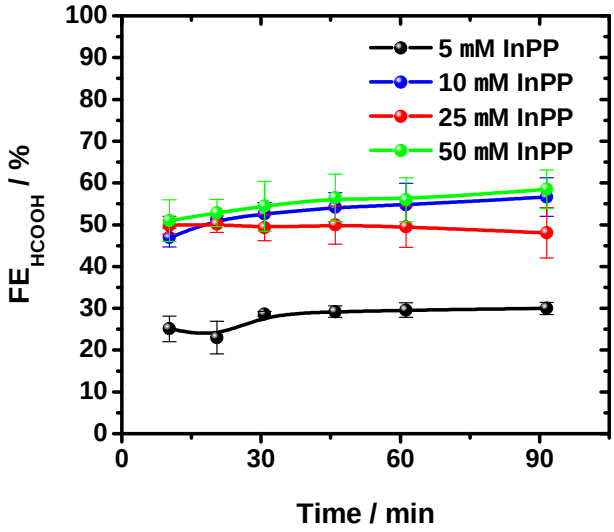

Figure S4: Faradaic efficiency toward HCOOH during CO_2 reduction on PG in phosphate buffer of pH $\approx$ 9.6 containing different concentrations of InPP. Lines to guide the eye.

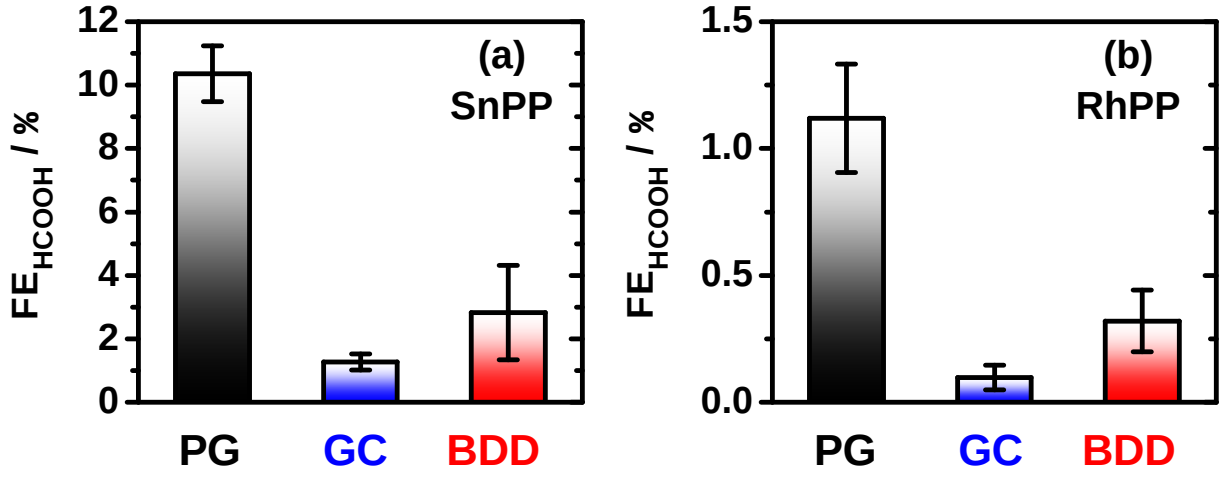

Figure S5: Faradaic efficiency toward HCOOH during CO_2 reduction at E = -1.5 V vs. RHE in 0.1 M phosphate buffer of pH 9.6 on (a) immobilized SnPP after 10 minutes, and (b) immobilized RhPP after 30 minutes on different substrates.

Pretreatment effect

In Figure S6 the CO_2RR performance of O_2 plasma treated PG with different exposure time is compared. The FE decreases, and j_{H_2} increases for 12 minutes O_2 plasma treatment. J_{total} does not show a clear trend as a function of exposure time. In Figure S7 we characterize the PG surface before and after pretreatment, by means of cyclic voltammetry. Significant difference is observed with the anodic treatment, whereas the other treatments lead to similar voltammograms. This observation is in agreement with the increased double layer capacitance shown in Figure S8(b).

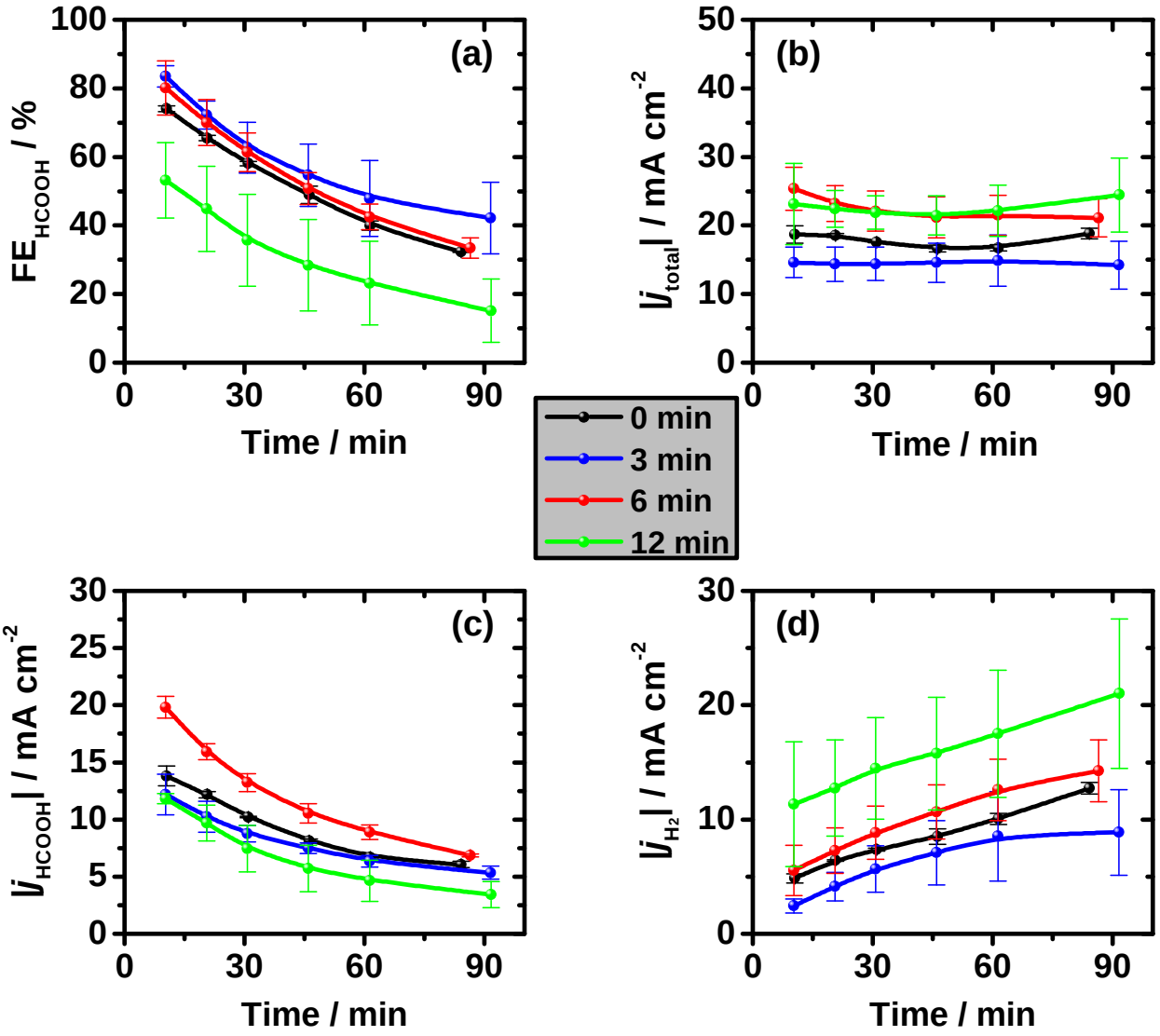

Figure S6: (a) Faradaic efficiency toward HCOOH, (b) Absolute total current density, (c) Absolute partial current density for HCOOH (d) Absolute partial current density for CO_2 reduction on immobilized InPP on PG with different exposure times of O_2 plasma in 0.1 M phosphate buffer of pH 9.6. Lines to guide the eye.

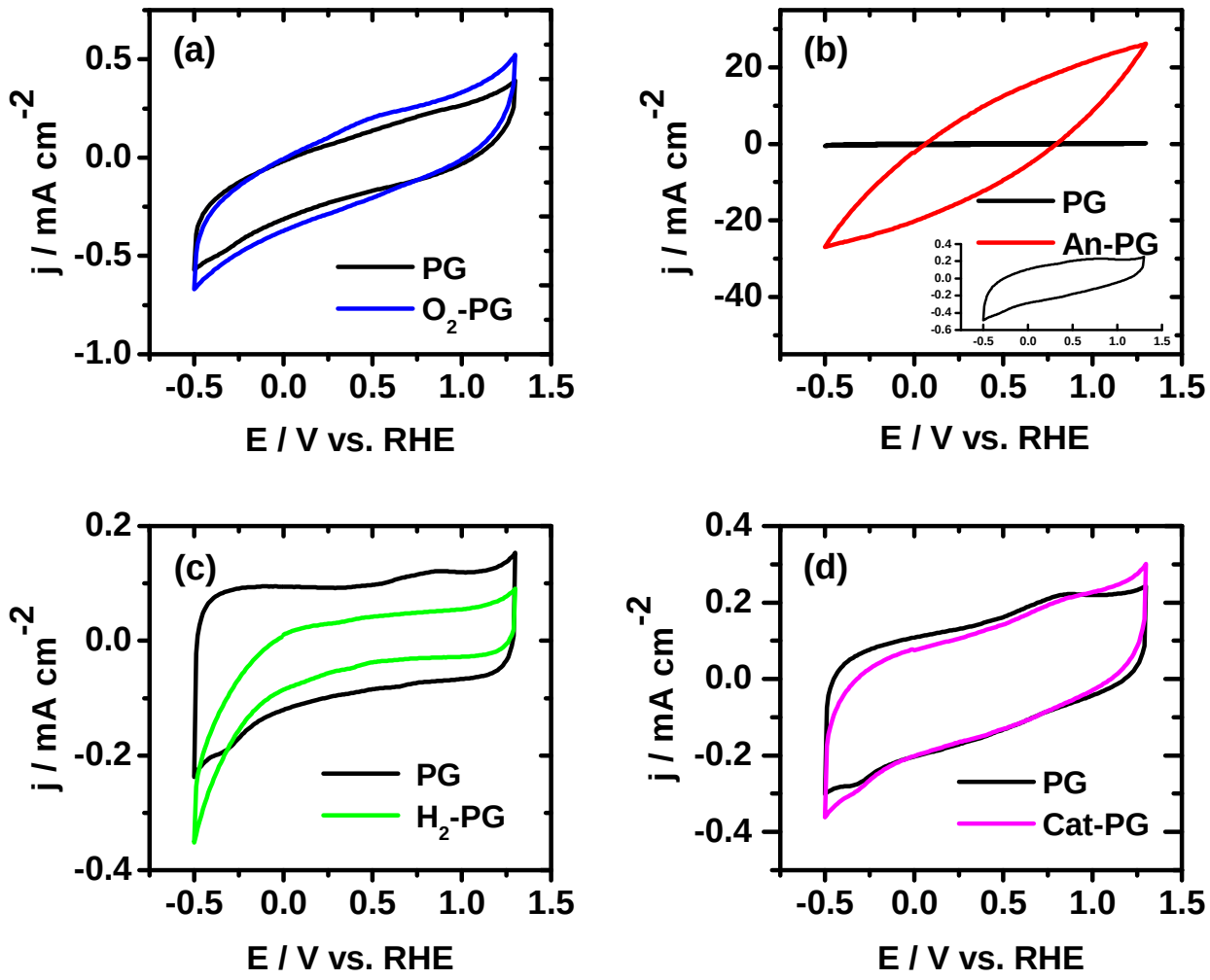

Figure S7: Blank voltammograms before and after pretreatment of PG: (a) O_2 plasma treatment (6 min), (b) Anodic treatment, (c) H_2 plasma treatment, (d) Cathodic treatment. Electrolyte: 0.1 M phosphate buffer of pH 9.6. Scan rate: 500 mV s^{-1}

Characterization

In Figure S8, the double layer capacitance (C_{dl}) in μF cm^{-2} is shown for the investigated substrates, and pretreated PG. C_{dl} is derived from voltammograms measured in the double layer region at different scan rates. The slope of I vs. scan rate at a fixed potential is the capacity, which is normalized by the geometric area of the electrode. C_{dl} is proportional to the electrochemical active surface area or roughness of the electrode ($C = \frac{\epsilon A}{d}$). The ratio between C_{dl} of the investigated substrates is different from the ratio between j_{total} of the investigated substrates (Figure 1(b)), which indicates that the difference in activity observed between the substrates is not the result of a difference in active surface area.

The XRD patterns for the investigated substrates, electrochemical pretreated PG, and polymer coated PG are shown in Figure S9. The electrochemical pretreatments and InPP encapsulation in polymers do not affect the crystallinity of the PG.

In Figure S10a, the Raman spectra are depicted for the investigated substrates PG, GC, and BDD revealing the peaks related to the sp^2 (D, G, 2D) and sp^3 carbon atoms. The peak at 1330 cm^{-1} observed in BDD is associated to the σ bonds between the C atoms. Graphite shows the G-band at 1580 cm^{-1}, which is characteristic for crystalline graphite (hence GC exhibits a weak and broad G-band), and the D-band at 1352 cm^{-1}, which is typically assigned to disorder of the graphite lattice by edge planes. It should be noted that discrimination of the D-band with the sp^3 carbon peak is difficult in case a laser with a wavelength of 632 nm is used. Hence we used a laser with a wavelength of 532 nm. The peaks between 2400 and 3300 cm^{-1} are second order features attributed to overtones of fundamental modes.[5] Figure S10b shows the Raman spectra for PG and after the various pretreatments. Based on the intensities obtained here for the D and G peaks, the ratios of I_D/I_G are depicted in Figure S11.

As discussed before, XPS measurements were carried out to obtain more quantitative information about the surface species. The indium content is used to compare the real amount of indium adsorbed on the various substrates, and to compare the stability between

the different substrates. Additionally, the oxygen content is used to provide a quantitative basis for the conclusions related to the pretreatment effect.

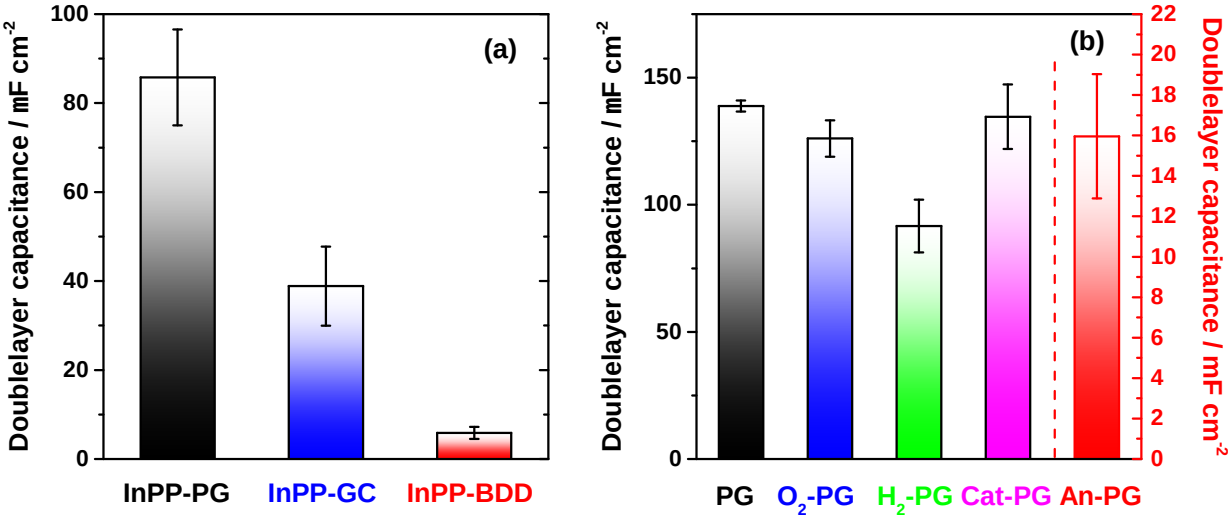

Figure S8: Double layer capacitance of (a) investigated substrates and (b) different pretreatments of PG.

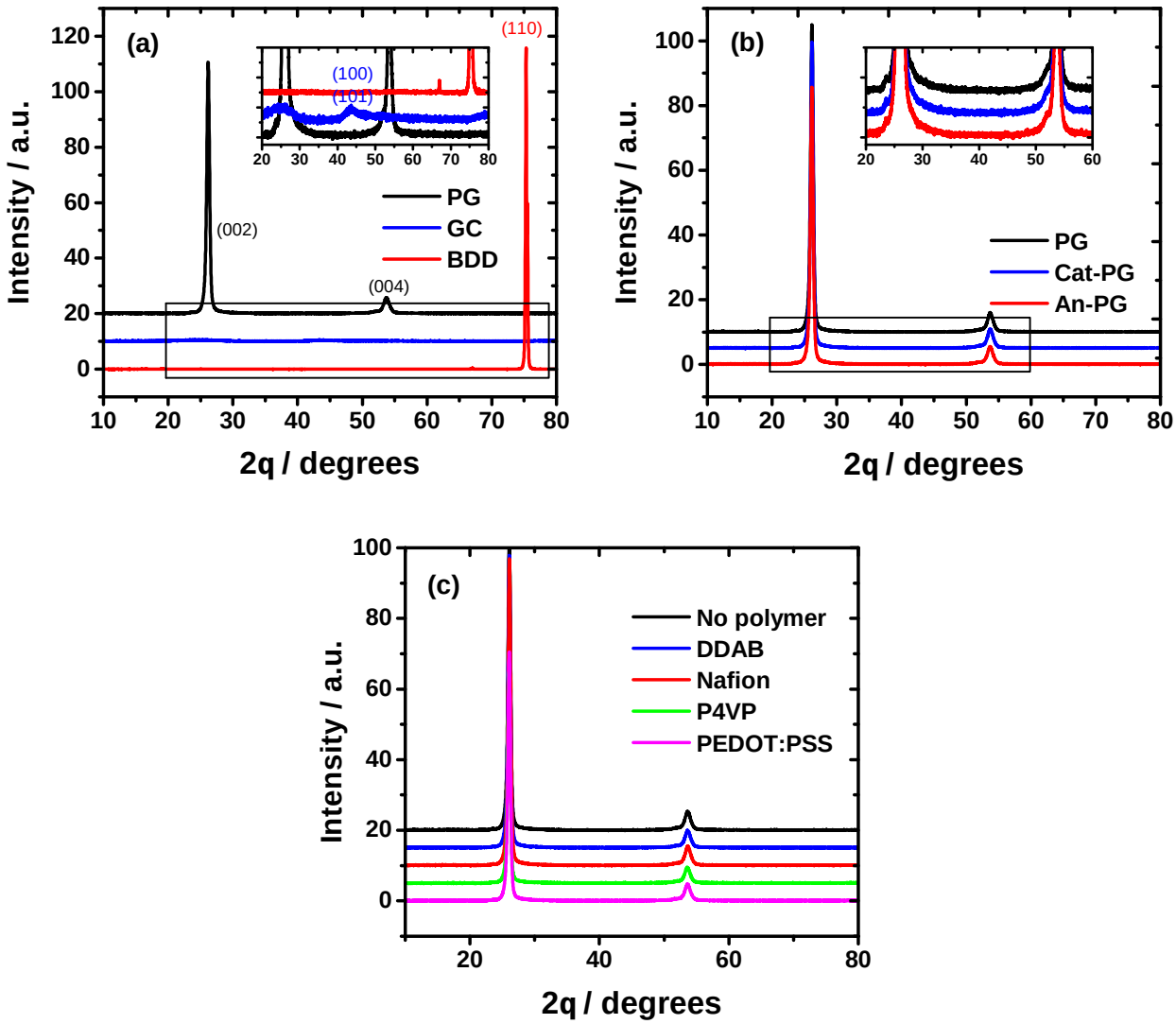

Figure S9: XRD patterns of (a) different substrates, (b) untreated, anodically treated and cathodically treated PG and (c) PG coated with InPP in different polymer films.

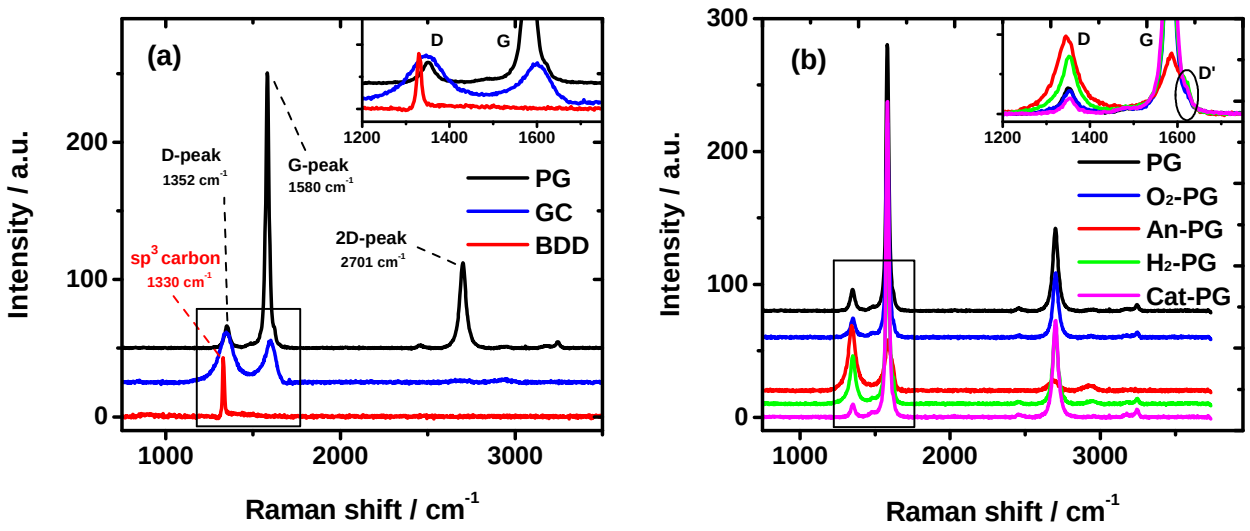

Figure S10: Raman spectra of (a) the different substrates and (b) the different pretreatments of PG.

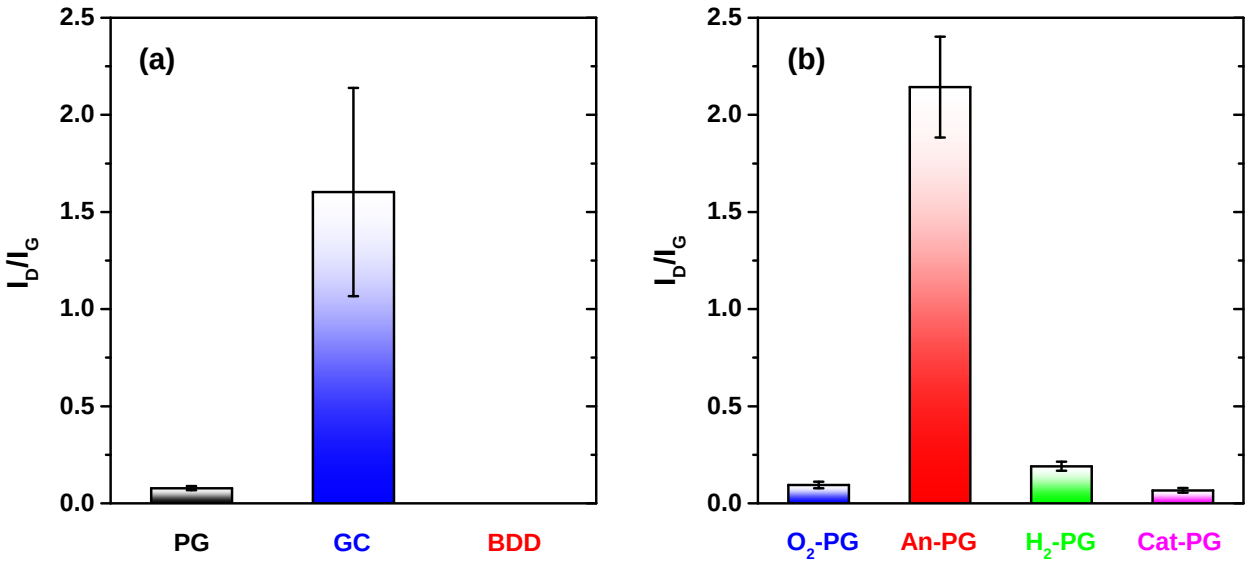

Figure S11: Ratio of D-peak and G-peak intensity of (a) the different substrates and (b) the different pretreatments of PG.

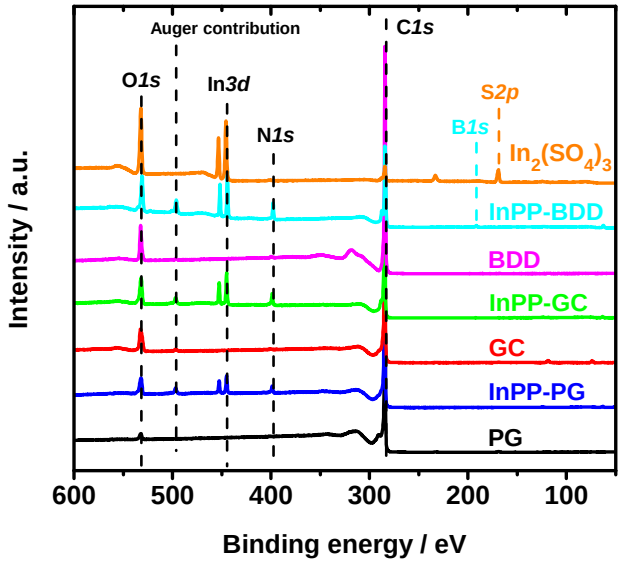

Figure S12: XPS spectra of the different substrates with and without immobilized InPP, and $In_2(SO_4)_3$.

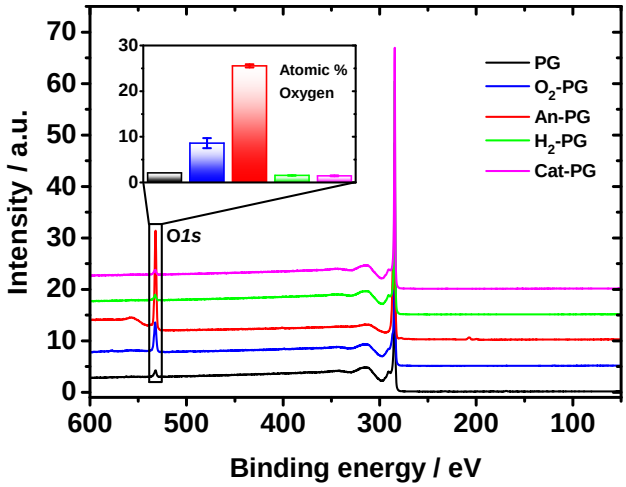

Figure S13: XPS spectra of plasma- and electrochemically pretreated pyrolytic graphite. Inset: comparison of the oxygen content (at.%) between the pretreated PG.

Effect of polymer encapsulation

In Figure S14, the chemical structures of the investigated polymers are depicted. In Figure S15, we compare the blank cyclic voltammograms of InPP immobilized on PG using different polymers. The typical peaks observed after InPP immobilization without polymer or with DDAB (denoted by the arrows) are not always visible (P4VP and Nafion), possibly due to a shift of the redox peaks as observed before.[4] In case of PEDOT:PSS a larger double layer and additional peaks are observed, which is assumed to be related with the polymer chemical structure. The differences in the CVs are believed to be the result of a different chemical environment in vicinity of the electrode as observed before.[4]

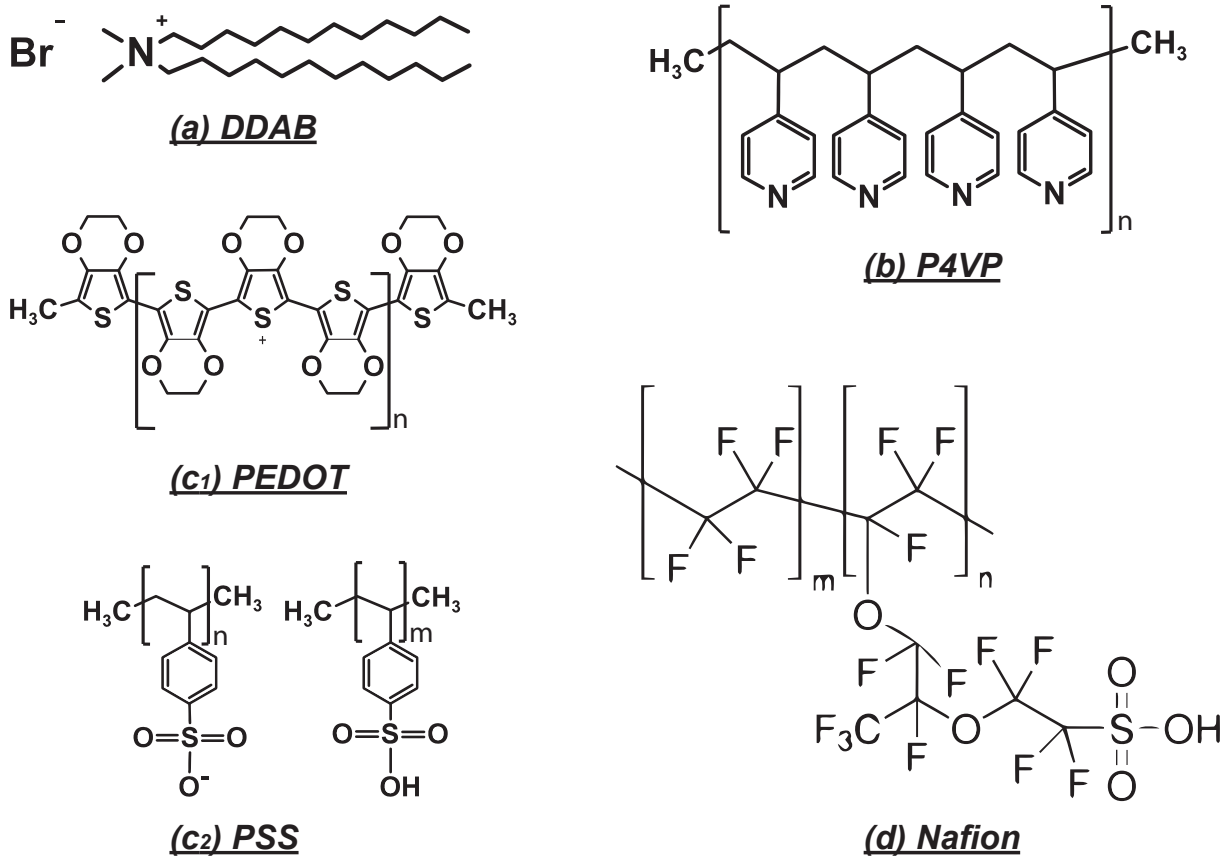

Figure S14: Chemical structures of the investigated polymers for InPP immobilization: (a) DDAB, (b) P4VP, (c) PEDOT:PSS and (d) Nafion

We performed Electrochemical Impedance Spectroscopy experiments on the different

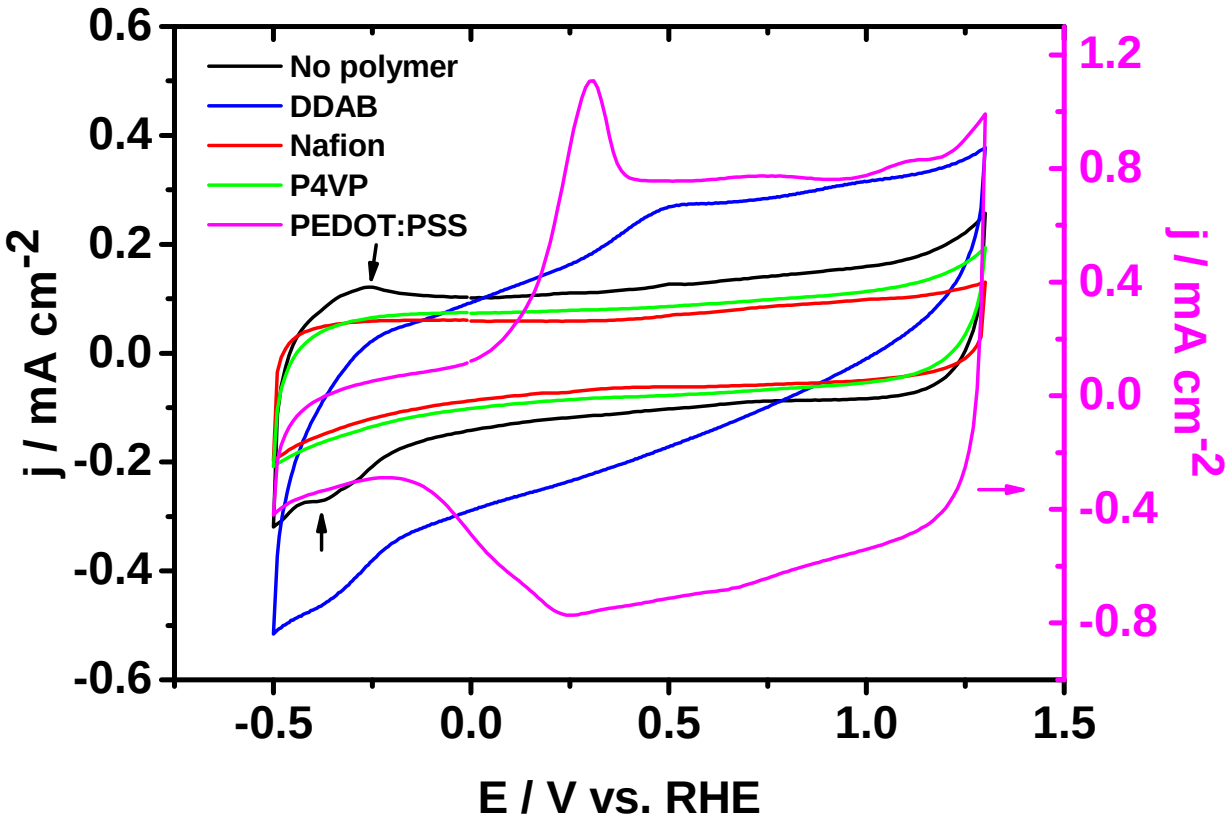

Figure S15: Blank voltammograms InPP immobilized on PG using different polymers. Electrolyte: 0.1 M phosphate buffer of pH 9.6. Scan rate: 500 mV s^{-1}

polymer dispersed catalysts to investigate the kinetics of electron-transfer processes. The Nyquist plots were obtained in CO_2-saturated and blank (argon saturated) 0.1 M phosphate buffer solution of pH 9.6 in a frequency range from 10 kHz to 1 Hz with an amplitude of 10 mV at a potential of -1.5 V vs. RHE, similar to the potential at which we performed the CO_2RR electrolysis experiments. From the Nyquist plots (Figure S16a-b), we observe only one semicircle, and the absence of a mass transfer controlled regime, which generally indicates that the impedance is determined by slow electron transfer kinetics. The diameter of the semicircle is a measure of the charge transfer resistance (R_{ct}), which is different for the various polymer films and different in the blank vs. CO_2 saturated electrolyte. The data is fitted with typical Randles equivalent circuits in series, modified by replacing the capacitor with a constant phase element and omitting the diffusion element (Figure S16c), which leads to a better fit for our data, and which has been used for polymer-modified electrodes.[6,7] Fit-

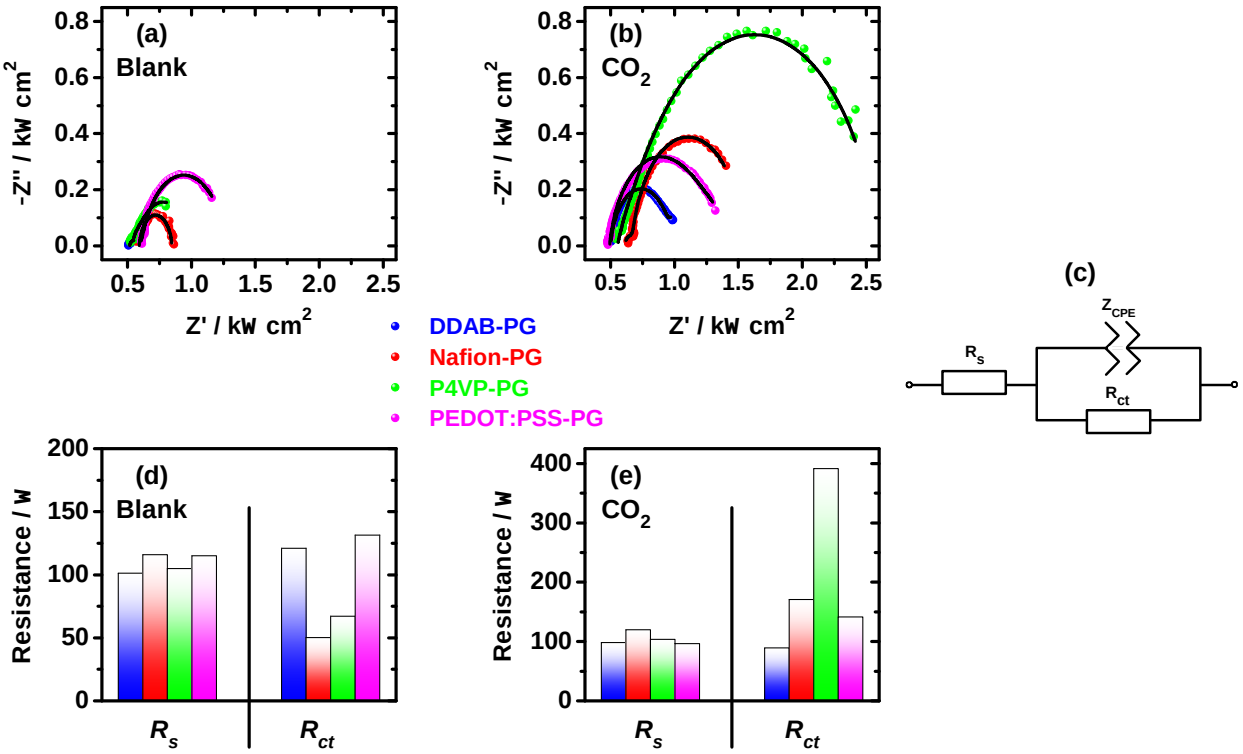

Figure S16: Nyquist impedance plots of polymer encapsulated InPP on PG in (a) argon-purged, and (b) CO_2-purged electrolyte in a frequency range of 10 kHz to 1 Hz with 10 mV amplitude at E = -1.5 V vs. RHE. (c) a single (modified) Randles equivalent circuit. Parameters of the fitted equivalent circuit in (d) argon-purged, and (e) CO_2-purged solution: solution resistance (R_s) in the left panels and charge transfer resistance (R_{ct}) in the right panels.

ting was performed with the software provided by potentiostat manufacturer (IviumSoft). We also tried more complex equivalent circuits reported in the literature, which turned out to be incompatible with our Nyquist plots due to the absence of a diffusion controlled region.[8,9]

The relevant fitting parameters obtained, are the ohmic bulk solution resistance (R_s), charge transfer resistance (R_{ct}), and double layer capacitance (C_{dl}). C_{dl} values were not included in the analysis, since EIS was measured at potentials much more negative than the double layer region. Hence, the C_{dl} values obtained in Figure S8 are more accurate. In Figure S16 d-e, we plotted the obtained values of R_s (left panels) and R_{ct} (right panels) in blank and CO_2-purged electrolyte for the different polymer films.

R_s is found to be similar between the different polymers, which is expected since the

electrolyte composition is unchanged. Furthermore, the difference in R_s between the polymers does not affect the CO_2RR performance, since we corrected for Ohmic drop during electrolysis. The relevant parameter is the charge transfer resistance (R_{ct}). It can be seen from the right panels in Figures S16c-d, that R_{ct} is increased under CO_2 atmosphere for all polymers, which indicates a lower rate of electron transfer for CO_2RR compared to HER. Additionally, we observe a relatively high R_{ct} for P4VP under CO_2 atmosphere, indicating a lower electron transfer rate, which is in agreement with the lower current density observed for P4VP in Figure 6b. The trend of R_{ct} between the polymers is in line with the current density for the different polymers, but given the single semicircle nature of the EIS data, the additional information obtained from the EIS with respect to the CV data is unfortunately very limited. From these results, we conclude that the nature of the polymer affects the rate of electron transfer during CO_2RR rather than mass transport of active species, leading to different activity. Note that this EIS analysis does not allow us to draw conclusions about the difference in CO_2RR selectivity between the different polymers used for encapsulation of InPP.

Control experiments

For a correct ascription of the observed substrate effects and influence of polymer encapsulation, control experiments were performed. CO_2 reduction was investigated under the same conditions, but without InPP present. The faradaic efficiency after 20 minutes is shown in Figure S17. As can be seen in Figure S17a, PG exhibit little activity for CO_2RR (FE $< 4\%$), while GC and BDD are not active for CO_2RR (FE $< 0.5\%$).

In Figure S17b, it can be seen that the polymer itself is active for CO_2RR. This trend is comparable with the mutual differences in FE observed in Figure 6. Therefore we believe that the influence of the polymer is partly caused by the intrinsic activity of the polymer towards HCOOH.

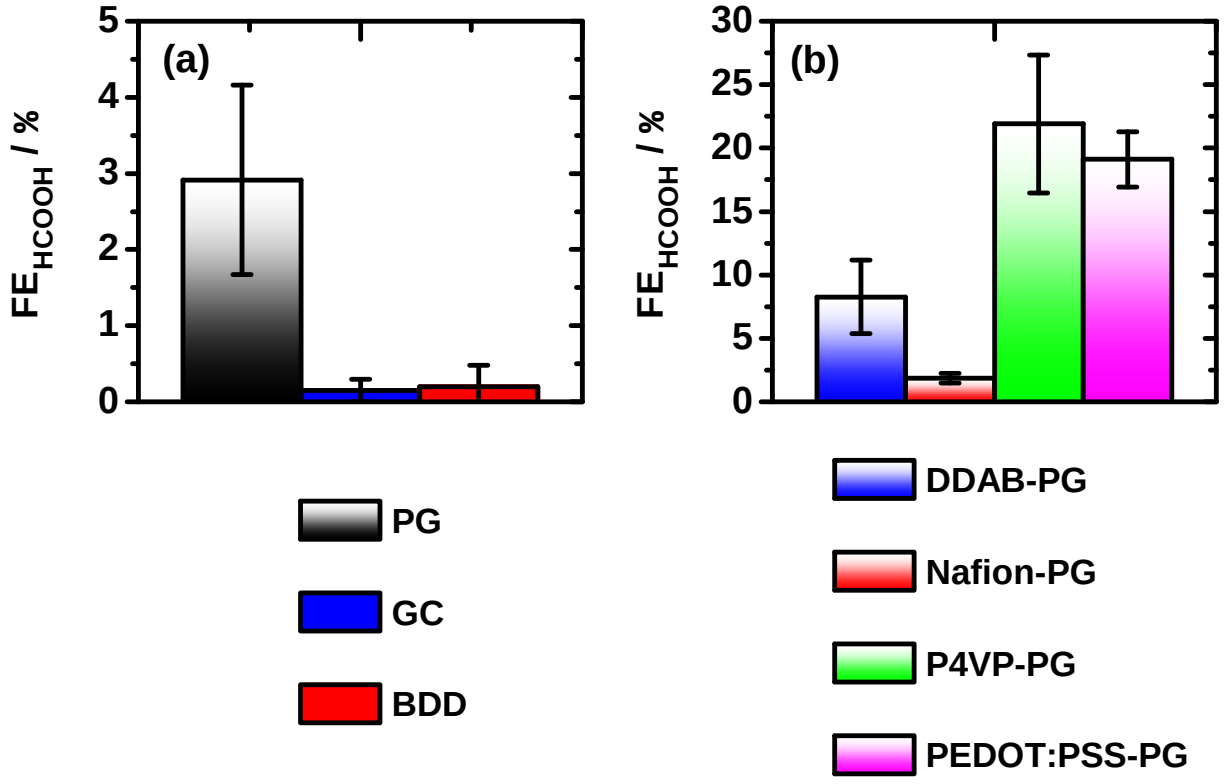

Figure S17: Control experiments for (a) the substrate effect and (b) the effect of polymer encapsulation

References

(1) Birdja, Y. Y.; Shen, J.; Koper, M. T. M. Influence of the metal center of metalloprotoporphyrins on the electrocatalytic CO_2 reduction to formic acid. *Catal. Today* **2017**, *288*, 37–47.

(2) Kwon, Y.; Koper, M. T. M. Combining Voltammetry with HPLC: Application to Electro-Oxidation of Glycerol. *Anal. Chem.* **2010**, *82*, 5420–5424.

(3) Wonders, A. H.; Housmans, T. H. M.; Rosca, V.; Koper, M. T. M. On-line mass spectrometry system for measurements at single-crystal electrodes in hanging meniscus configuration. *J. Appl. Electrochem.* **2006**, *36*, 1215–1221.

(4) de Groot, M.; Koper, M. T. M. Redox transitions of chromium, manganese, iron, cobalt and nickel protoporphyrins in aqueous solution. *Phys. Chem. Chem. Phys.* **2008**, *10*, 1023–1031.

(5) Wang, Y.; Alsmeyer, D. C.; McCreery, R. L. Raman Spectroscopy of Carbon Materials: Structural Basis of Observed Spectra. *Chem. Mater.* **1990**, *2*, 557–563.

(6) Bisquert, J.; Garcia-Belmonte, G.; Bueno, P.; Longo, E.; Bulhões, L. Impedance of constant phase element (CPE)-blocked diffusion in film electrodes. *J. Electroanal. Chem.* **1998**, *452*, 229–234.

(7) Chen, Z.; Yao, S.; Liu, L. 3D hierarchical porous structured carbon nanotube aerogel-supported Sn spheroidal particles: an efficient and selective catalyst for electrochemical reduction of CO_2 to formate. *J. Mater. Chem. A* **2017**, *5*, 24651–24656.

(8) Sharp, M.; Lindholm-Sethson, B.; Lind, E.-L. An impedance spectroscopy study of charge propagation in Nafion films containing discrete redox sites. *J. Electroanal. Chem.* **1993**, *345*, 223–242.

(9) Calfumán, K.; Honores, J.; Guzmán, D.; Ohlbaum, M.; Armijo, F.; Río, R. D.; Isaacs, M. Electrochemical Conversion of Carbon Dioxide into CHO-Containing Compounds on Multimetallic Porphyrins. *ChemElectroChem* **2017**, *4*, 3314–3321.